Relation between the structural phase transition and superconductivity in $Cu_xIrTe_{2-y}Se_y$

M. Kamitani,[1,*] H. Sakai,[1,†] Y. Tokura,[1,2] and S. Ishiwata[1,3]
[1]*Department of Applied Physics, University of Tokyo, Hongo, Tokyo 113-8656, Japan*
[2]*RIKEN Center for Emergent Matter Science (CEMS), Wako 351-0198, Japan*
[3]*JST, PRESTO, Kawaguchi, Saitama 332-0012, Japan*
(Received 15 April 2016; revised manuscript received 30 August 2016; published 12 October 2016)

We have investigated the relation between structural transition with Ir-dimer formation and superconductivity in $IrTe_2$ by combining the Se substitution and the Cu intercalation. Regardless of the structural transition temperature (T_s), which increases with increasing the Se content (y) in $IrTe_{2-y}Se_y$, superconductivity emerges robustly by the Cu intercalation. As the Cu content x in $Cu_xIrTe_{2-y}Se_y$ increases, T_s tends to decrease, followed by the emergence of superconductivity with showing the highest critical temperature (T_c) at the optimum Cu concentration (x_{opt}) close to the structural phase boundary. Based on the transport and thermodynamic properties, the electron-phonon coupling constant is found to be enhanced near the structural phase boundary, which suggests an essential role of the structural instability for the superconductivity in doped $IrTe_2$. With increasing y from 0 to 0.5 in $Cu_xIrTe_{2-y}Se_y$, T_s at $x = 0$ increases by about 80%, whereas T_c at $x = x_{opt}$ decreases by about 20%. This can be understood by the weakening of the interlayer hybridization upon the Se substitution, resulting in the weak but negative correlation between T_s and T_c through y.

DOI: 10.1103/PhysRevB.94.134507

I. INTRODUCTION

Recently, $IrTe_2$ with CdI_2-type structure has received great attention because of a unique superconductivity possibly with large spin-orbit coupling [1–3]. $IrTe_2$ with trigonal symmetry at high temperatures undergoes a first-order structural phase transition at around 250 K while holding metallic conductivity [4]. The low-temperature phase was initially reported to have monoclinic symmetry with uniform charge density, followed by a seminal work suggesting a charge density wavelike state with a modulation vector $\mathbf{q} = (1/5,0,-1/5)$ [1]. By single-crystal x-ray diffraction, the charge density modulation was revealed to be nonsinusoidal, viewed as a periodic arrangement of Ir dimers [5–7]. As an origin of the structural transition, a band Jahn-Teller effect promoting the Ir dimerization has been proposed [8,9], whereas the important role of Te p orbitals has been pointed out [3,10–12].

As for the superconductivity in doped $IrTe_2$, while the origin has been discussed in terms of simple BCS mechanism [2,13], its relation to the Ir dimer formation remains elusive. Kiswandhi *et al.* studied the pressure effect on $Ir_{1-x}Pt_xTe_2$ up to 1 GPa and found a competitive nature between the structural and superconducting transitions [13]. To understand the underlying physics of doped or intercalated $IrTe_2$ superconductors, it is essential to clarify the relation between the Ir dimer formation and the superconductivity by tuning their transition temperatures to a large extent. For this purpose, $IrTe_2$ with Se substitution and Cu intercalation appears to be an ideal system, since the Se substitution significantly enhances the structural transition temperature (T_s) with changing the superlattice modulation from $\mathbf{q} = (1/5,0,-1/5)$ (denoted as 1/5 stripe) to $\mathbf{q} = (1/6,0,-1/6)$ (denoted as 1/6 stripe) with the highest Ir-dimer density [10], and the superconductivity is expected to be stabilized by the Cu intercalation without chemical disturbance for the Ir site.

In this study we report on the systematic investigation of the structural and electronic properties of Cu intercalated $IrTe_{2-y}Se_y$. While T_s of the Cu-free compound $IrTe_{2-y}Se_y$ increases up to more than 400 K for $y = 0.6$, superconductivity emerges in the Cu-intercalated compounds $Cu_xIrTe_{2-y}Se_y$ in the vicinity of the structural phase boundary, of which T_c at the optimum composition tends to decrease slightly with increasing y. We show the global electronic phase diagram for $Cu_xIrTe_{2-y}Se_y$ to clarify the relation between the structural phase transition and superconductivity. Based on the systematic thermodynamic measurements, we also discuss the role of electron-phonon coupling that appears to be enhanced by suppressing the Ir dimerization.

II. EXPERIMENT

Polycrystalline samples of $Cu_xIrTe_{2-y}Se_y$ were synthesized in the same manner as reported previously [3]. The samples were characterized by the powder x-ray diffraction technique with a Cu $K\alpha$ radiation. Here let us comment on the solubility limit. In our samples, small impurity phases were discerned above $y = 0.8$ for $IrTe_{2-y}Se_y$. On the other hand, the intercalation limit of Cu for Cu_xIrTe_2 is $x = 0.1$, and that for $Cu_xIrTe_{2-y}Se_y$ ($y = 0.2, 0.3, 0.5$) extends up to $x = 0.2$. The reflections of the low-temperature phases, which have triclinic supercells, were indexed by a monoclinic unit cell ($C2/m$) with ignoring superlattice modulations (thus we call the low-temperature phase monoclinic phase). In order to see the systematic change in the lattice parameters of the monoclinic and the trigonal phases as a function of x, the lengths of a axis and c axis in the monoclinic structure [4,10,14] are converted to those of the trigonal phase ($P-3m1$) as $a' = \sqrt{2(V_{mono}/Z)/(\sqrt{3}c')}$ and $c' = c_{mono}\sin(\beta)$, where V_{mono}/Z is

*Present address: RIKEN Center for Emergent Matter Science (CEMS), Wako 351-0198, Japan; kamitani@ce.t.u-tokyo.ac.jp; manabu.kamitani@riken.jp
†Present address: Department of Physics, Osaka University, Toyonaka, Osaka 560-0043, Japan; sakai@phys.sci.osaka-u.ac.jp

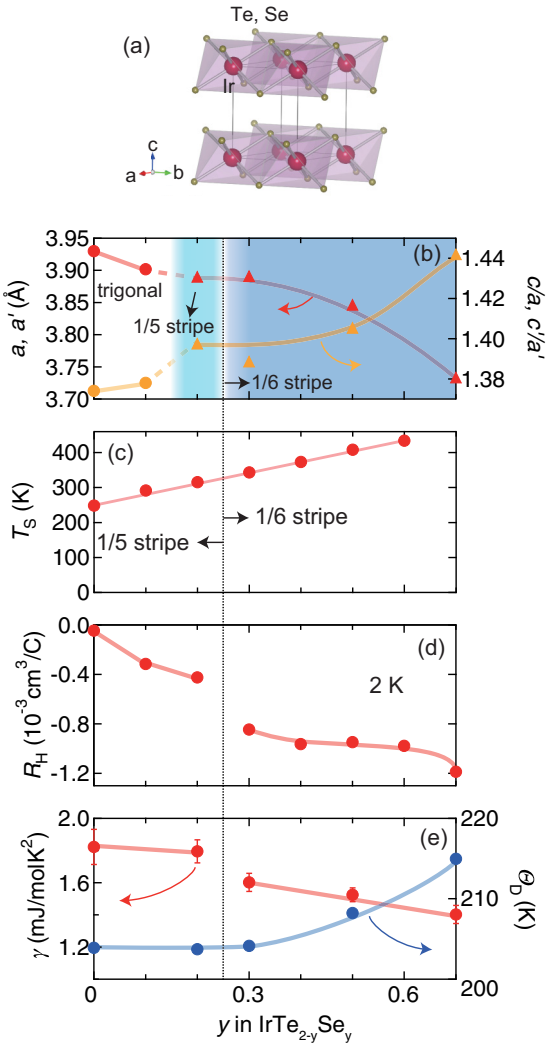

FIG. 1. (a) Crystal structure of $IrTe_2$. (b) Variation of in-plane (a, a') lattice constant and lattice anisotropy ratio (c/a, c'/a') of $IrTe_{2-y}Se_y$. a' and c' represent the in-plane and out-of-plane lattice parameters of the pseudotrigonal cell converted from the monoclinic cell (see the main text for detailed definitions), respectively. Solid and dashed lines are guides to the eyes. (c) Variation of T_s as a function of y. Solid line is a guide to the eye. (d) Hall coefficient at 2 K for $IrTe_{2-y}Se_y$ obtained by linear fitting of Hall resistivity vs magnetic field data. (e) Electronic specific-heat coefficient γ (left) and Debye temperature Θ_D (right) as a function of y. Black dotted line in (b)–(e) is a boundary separating the 1/5 and 1/6 stripe phases. Solid lines in (d) and (e) are merely guides to the eyes.

the volume per formula unit and β is the monoclinic angle. The electrical resistivity, Hall resistivity, and specific heat were measured with Physical Property Measurement System (PPMS, Quantum Design).

III. RESULTS AND DISCUSSION

A. Lattice parameters and electronic properties of $IrTe_{2-y}Se_y$

We first show the Se doping effect on the lattice parameters at room temperature and the first-order structural transition temperature T_s of $IrTe_2$. As shown in Fig. 1(b), the a-axis length of $IrTe_{2-y}Se_y$ decreases with increasing y up to 0.7, reflecting the smaller ionic radius of Se than that of Te. On the other hand, the c/a ratio increases upon the Se doping, accompanied by a sharp increase at the structural transition from the trigonal phase to the monoclinic phase. The c/a ratio is a good indicator for the strength of the interlayer hybridization in layered transition metal dichalcogenides [10,15]. The c/a ratio for $IrTe_2$ is much smaller than the value 1.633 for the system with ideal van der Waals stacking. The significant reduction of the c/a ratio in $IrTe_2$ reflects the strong interlayer hybridization via p_z orbitals [15]. Thus, the increase of the c/a ratio from 1.38 for $IrTe_2$ to 1.44 for $IrTe_{1.3}Se_{0.7}$ indicates the weakening of the interlayer hybridization. Figure 1(c) shows the Se content dependence of T_s for $IrTe_{2-y}Se_y$. T_s is defined as the value averaged over the two transition temperatures on cooling and warming (see Fig. 3), where $d\rho/dT$ take minima. T_s of $IrTe_{2-y}Se_y$ shifts markedly to higher temperature as the Se content increases as reported in a previous work [10] [see the data for $x = 0$ in Figs. 3(a)–3(d)]. To be noted here is that the single crystal of $IrTe_2$ obtained after slow cooling was reported to show two thermal transitions, one of which at lower temperature corresponds to the reordering from the 1/5 stripe to the 1/8 stripe phase with higher Ir-dimer density [16,17]. For our samples, since there exists only one transition in each temperature profile, we here presume that there is no thermal reordering of Ir dimers. Considering the experimental fact that the Se doping effect on lattice parameters and T_s are consistent with the previous work [10], however, there should be a change from the 1/5 stripe to the 1/6 stripe phase at somewhere between $y = 0.2$ and 0.3 as reported in Refs. [10,17].

To see how the electronic state of the low-temperature monoclinic phase in $IrTe_{2-y}Se_y$ depends on the Se content y ($0 \leqslant y \leqslant 0.7$), we carried out Hall resistivity measurements [18]. Figure 1(d) presents the Se content (y) dependence of Hall coefficient (R_H) at 2 K. The magnitude of R_H at 2 K increases with increasing y up to 0.7, indicating a systematic change in the band structure near the Fermi level (E_F). Note that R_H shows a discontinuous change around $y = 0.2$–0.3. This behavior implies the reconstruction of the Fermi surface on going from the 1/5 stripe to the 1/6 stripe phase, as will be discussed later.

The systematic change of the electronic state by the Se substitution is confirmed also by specific heat measurements (raw data of the temperature dependence of specific heat is given in Fig. S2 of the Supplemental Material [18]). The electronic specific heat coefficient γ and Debye temperature Θ_D are estimated by applying the conventional relation $C/T = \gamma + \beta T^2$ to the specific heat data in the temperature range between 2 and 10 K, where Θ_D equals $(12\pi^4 Rn/5\beta)^{1/3}$ with R and n, respectively, denoting the gas constant and number of atoms per formula unit. As shown in Fig. 1(e), γ tends to decrease upon the Se doping, which suggests a slight reduction of the density of states (DOS) near E_F. The reduction of DOS on increasing the Se content y from 0 to 0.7 is ascribable to the weakening of the interlayer coupling mediated by the chalcogen p_z orbitals, since the energy level of the top of antibonding p bands (mainly p_z band) near E_F in CdI_2-type MTe_2 generally shifts to lower energy by the Se substitution [19,20]. This explanation is consistent with the systematic

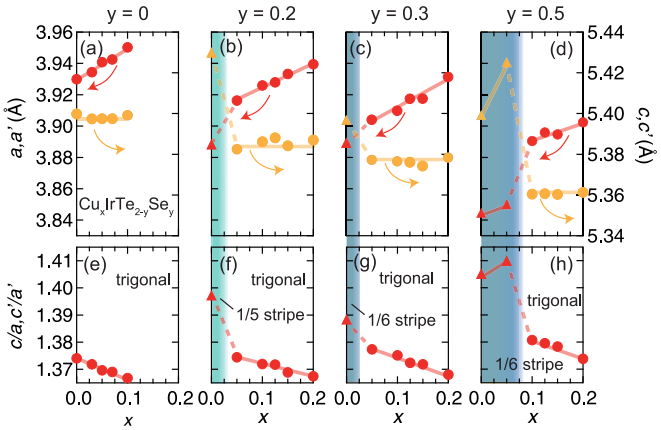

FIG. 2. Variation of the in-plane (a, a') and out-of-plane (c, c') lattice constants for (a) $y = 0$, (b) $y = 0.2$, (c) $y = 0.3$, and (d) $y = 0.5$ as a function of x in $Cu_xIrTe_{2-y}Se_y$. Lattice anisotropy ratio (c/a, c'/a') for (e) $y = 0$, (f) $y = 0.2$, (g) $y = 0.3$, and (h) $y = 0.5$ as a function of x. Filled triangles and circles correspond to the lattice parameters of the monoclinic phase and the trigonal phase, respectively. Solid and dashed lines are guides to the eyes.

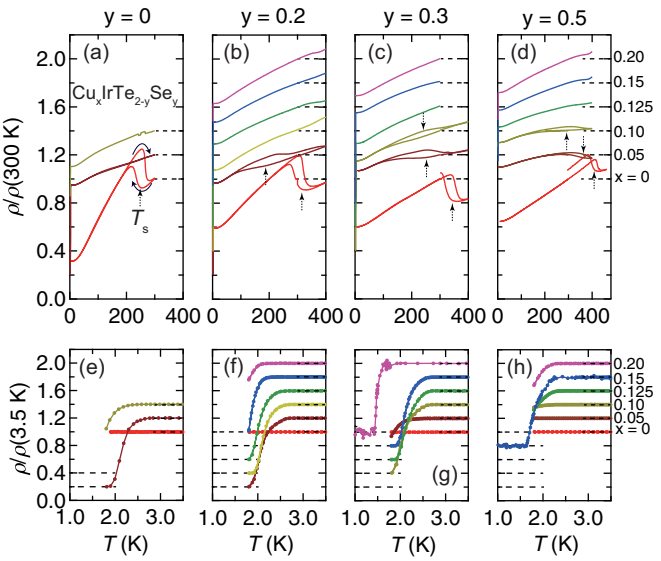

FIG. 3. Temperature dependence of normalized resistivity $\rho/\rho(300\ \mathrm{K})$ of $Cu_xIrTe_{2-y}Se_y$ with x ($0 \leqslant x \leqslant 0.20$) for (a) $y = 0$, (b) $y = 0.2$, (c) $y = 0.3$, and (d) $y = 0.5$. Temperature dependence of $\rho/\rho(3.5\ \mathrm{K})$ for (e) $y = 0$, (f) $y = 0.2$, (g) $y = 0.3$, and (h) $y = 0.5$ under zero magnetic fields. Black dotted arrows indicate the structural phase transition temperature (see the detailed definition described in the text). For Cu doped samples, the data are shifted by 0.2 for clarity. Black curved arrows marked for $IrTe_2$ indicate the warming and cooling processes. For samples without showing the first-order phase transitions, we show only the data collected on warming.

increase in c/a by the Se substitution [see Fig. 1(b)]. The positive correlation between Θ_D and y in the range $y \geqslant 0.3$ likely reflects the decrease of the averaged weight of the chalcogen ion.

On increasing y from 0.2 to 0.3, where R_H shows a discontinuous change upon the reordering of the Ir dimers, there can be seen slight drops in γ [Figs. 1(d) and 1(e)]. It is predicted from the band calculations that the formation of Ir dimers causes bonding-antibonding splitting in a part of d bands located near E_F [5,6]. With the result of the band calculations taken into consideration, we interpret the drop in γ as a manifestation of the partial disappearance of the Fermi surface due to the increase of Ir dimers. This interpretation is consistent with the idea that the local lattice instability for the Ir dimer formation is a substantial driving force of the structural transition [5,6,8,16].

B. Lattice parameters of $Cu_xIrTe_{2-y}Se_y$

Figures 2(a)–2(d) show the variation of lattice parameters for $Cu_xIrTe_{2-y}Se_y$ ($0 \leqslant x \leqslant 0.2$, $0 \leqslant y \leqslant 0.5$). With increasing the Cu content x, the a-axis length for all the Se doped compounds shows a jump upon the transition from the monoclinic to the trigonal phase, followed by the gradual increase in the trigonal phase. In accord with the sharp increase in the a-axis length, the c-axis length and the c/a ratio show a dramatic decrease, suggesting that the interlayer hybridization between the chalcogen p orbitals is enhanced upon the transition to the trigonal phase. In the trigonal phase, the c/a ratio decreases as the Cu content x increases, indicating that the bonding between Cu d and chalcogen p orbitals is robustly formed in $Cu_xIrTe_{2-y}Se_y$. On the other hand, the gradual increase of c/a ratio upon the increase of y in the same x reflects the weakening of the interlayer coupling by the Se doping [see Figs. 2(e)–2(h)].

C. Emergence of superconductivity in $Cu_xIrTe_{2-y}Se_y$ and its electronic phase diagram

The temperature dependence of resistivity for $Cu_xIrTe_{2-y}Se_y$ ($0 \leqslant y \leqslant 0.5$) is shown in Figs. 3(a)–3(d). Irrespective of x and y, all the compounds show a metallic behavior in the measured temperature range. With increasing the Cu content x in $IrTe_{2-y}Se_y$, T_s decreases monotonically down to the critical values (x_s), where the structural phase boundary is located. As shown in Figs. 3(e)–3(h), a clear superconducting transition was observed in $\rho(T)$ of $Cu_xIrTe_{2-y}Se_y$ with y up to 0.5. For $y = 0.7$, no superconducting transition was detected at least down to 1.8 K upon the Cu doping up to $x = 0.2$ (data not shown). In Fig. 4, T_s and T_c(onset) determined from the resistivity measurements are summarized as a phase diagram as functions of x, y, and temperature. Robust emergence of superconductivity with domelike curves of T_c is confirmed near the structural phase boundary in the trigonal phase of Cu intercalated $IrTe_{2-y}Se_y$ up to $y = 0.5$. This result suggests that a strong competition between structural phase transition and superconducting transition remains intact irrespective of the Se content. The clear shielding signals corresponding to the superconducting volume fraction of about 10%–20% are also observed for the samples showing the zero resistivity above 1.8 K (not shown here). The superconductivity appears in the trigonal phase with x just above x_s. In fact, the values of x_{opt} are slightly larger than the values of x_s in the same y composition. With increasing the Se content y from 0 to 0.5, the optimum Cu content for superconductivity (x_{opt}) significantly increases

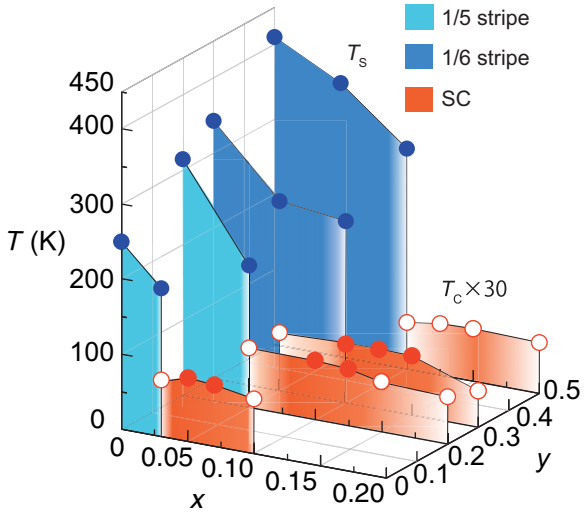

FIG. 4. Electronic phase diagram of $Cu_xIrTe_{2-y}Se_y$ as functions of x, y, and temperature. Blue filled circles indicate the critical temperatures for the structural phase transition averaged over the cooling and warming processes. Filled and open red circles denote the onset values of the superconducting transition temperature with zero resistivity above 1.8 K and ones with finite resistivity down to 1.8 K, respectively. The superconducting transition temperatures are multiplied by 30 for clarity.

from 0.05 to 0.15, whereas T_c at x_{opt} slightly decreases from 2.85 to 2.3 K. Considering the observation that T_s of the Cu free (parent) compound increases from 250 K ($y = 0$) to 410 K ($y = 0.5$), these results indicate that there is a weak but negative correlation between the structural transition temperature (T_s) of the parent compound and the T_c at x_{opt} for the Cu-intercalated compound in the same y.

D. Specific heat in $Cu_xIrTe_{2-y}Se_y$

To discuss the origin of superconductivity in $Cu_xIrTe_{2-y}Se_y$, we focus on the x dependence of the specific heat for $Cu_xIrTe_{2-y}Se_y$ with $y = 0$ and $y = 0.3$. Figures 5(a) and 5(b) show the temperature dependence of specific heat in the form of a C/T versus T^2 plot. Anomalies corresponding to the superconducting transition are less discernible for compounds with $y = 0.3$ than those for $y = 0$ in the T range down to 1.8 K, which reflects the slight decrease of T_c upon increasing the Se content y. Θ_D extracted from the normal state specific heat from 3 to 10 K for $y = 0$ and 0.3 is plotted as a function of x in Fig. 5(c). The value of Θ_D clearly shows a dip at x_{opt} for each y. The similar x dependence of Θ_D was observed for $Ir_{1-x}Pt_xTe_2$ [2], which might be indicative of the existence of low-lying soft phonons in the vicinity of the structural phase boundary. While the minimization of Debye temperature is confirmed with many data points in $Ir_{1-x}Pt_xTe_2$, the structural phase boundary is located at $x = 0.05$ in Cu_xIrTe_2, which is almost same value as that in $Ir_{1-x}Pt_xTe_2$ and $Ir_{1-x}Pd_xTe_2$. This fact supports the reliability of the chemical composition of our samples.

To further clarify the superconductivity stabilized near the structural phase boundary, we evaluate the electron-phonon coupling constant ($\lambda_{el\text{-}ph}$) from the following McMillan

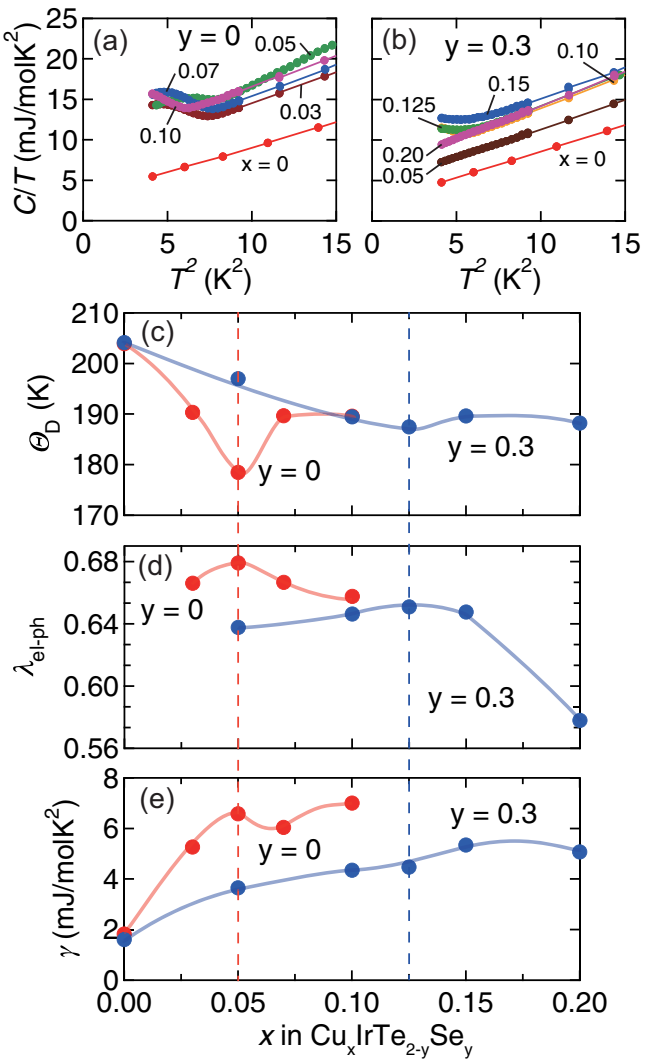

FIG. 5. Temperature dependence of specific heat C of $Cu_xIrTe_{2-y}Se_y$ for (a) $y = 0$ and (b) $y = 0.3$, plotted as C/T versus T^2. Cu content (x) dependence of (c) Debye temperature, (d) electron-phonon coupling constant, and (e) electronic specific heat coefficient of $Cu_xIrTe_{2-y}Se_y$. Filled red and blue circles indicate the data for $y = 0$ and $y = 0.3$, respectively. Vertical dashed lines correspond to the optimum composition (x_{opt}) for superconductivity of compounds with $y = 0$ (red) and $y = 0.3$ (blue). Solid lines in (c), (d), and (e) are guides to the eyes.

equation with T_c(onset) and Θ_D [21]:

$$\lambda_{el\text{-}ph} = \frac{1.04 + \mu^* \ln(\Theta_D/1.45T_c)}{(1 - 0.62\mu^*)\ln(\Theta_D/1.45T_c) - 1.04}. \quad (1)$$

Here μ^* denotes the Coulomb pseudopotential and we adopt a typical value 0.15 [22]. As shown in Fig. 5(d), $\lambda_{el\text{-}ph}$ of 0.6–0.7, which is comparable to that for typical weak coupling superconductors, takes maximum at x_{opt} for both $y = 0$ and 0.3. These results suggest that the enhanced electron-phonon coupling in the vicinity of the structural phase boundary plays an important role on the emergence of superconductivity in $Cu_xIrTe_{2-y}Se_y$, as suggested for other superconducting materials with structural instability [23–25]. We also apply the Bloch-Grüneisen equation to the temperature dependence of

resistivity for Cu_xIrTe_2 to derive $\lambda_{el\text{-}ph}$ (see the Supplemental Material for detailed discussion [18]). Enhancement of $\lambda_{el\text{-}ph}$ at the optimum composition $x = 0.05$ is roughly reproduced in this analysis, though the order of magnitude for $\lambda_{el\text{-}ph}$ deviates from that from McMillan equation. For $y = 0.3$, it seems that the drop of Θ_D and the resultant enhancement of $\lambda_{el\text{-}ph}$ near x_{opt} are weakened as compared to the system with $y = 0$. This observation implies that the Se doping reduces the electron-phonon coupling, which can be associated with the difference in the Ir-dimer ordering of the parent compounds of $y = 0$ and $y = 0.3$.

Now, let us consider the result of the x dependence of γ shown in Fig. 5(e). Unlike the x dependence of γ for $Ir_{1-x}Pt_xTe_2$ showing a sharp maximum at x_{opt}, that for $Cu_xIrTe_{2-y}Se_y$ with $y = 0$ and 0.3 shows an almost monotonic increase with x even above x_{opt}. Considering the experimental fact that the monotonic x dependence of γ for $Ir_{1-x}Pt_xTe_2$ in the trigonal phase is roughly consistent with a rigid band shift of the Fermi level [26], the x dependence of γ in $Cu_xIrTe_{2-y}Se_y$ allows us to consider an additional DOS at E_F, which cannot be described within a rigid band scheme. As the additional DOS in the trigonal phase, we presume a bond formation between Cu and chalcogen ions on the analogy of Cu_xTiSe_2, where the formation of Cu-Se bonds modifies the band structure of $TiSe_2$ [27]. In the trigonal phase of $y = 0.3$, the values of γ are lower than those in the trigonal phase of $y = 0$, which implies the decrease of the partial DOS for chalcogen p orbitals by Se doping in the Cu-intercalated compounds as well as the Cu-free compounds. The gradual decrease of T_c at x_{opt} with increasing the Se content y can be ascribed to the decrease of both $\lambda_{el\text{-}ph}$ and DOS at the optimum composition [28].

E. Relation between structural phase transition and superconductivity in $Cu_xIrTe_{2-y}Se_y$

Here let us discuss the relation between the structural phase transition and superconductivity in $Cu_xIrTe_{2-y}Se_y$. From the electronic phase diagram (Fig. 4), we have found a clear positive correlation between T_s and x_{opt} and a weak but negative correlation between T_s and T_c at x_{opt} with respect to the Se content y. Stabilization of the Ir-dimer formation by the Se substitution, which is confirmed by the enhancement of T_s with y in $IrTe_{2-y}Se_y$, can be ascribed to the weakening of interlayer Te-Te hybridization as suggested in [10]. On the other hand, the first-principles calculation revealed that the trigonal phase has stronger interlayer hybridization than that in the monoclinic phase with Ir dimers [3]. Thus, it is likely that with increasing the Se content the system requires higher Cu concentration to make interlayer hybridization strong enough to stabilize the trigonal phase, which results in an increase in x_s and x_{opt} as the Se content increases. Such a decrease in the interlayer hybridization by Se doping causes the decrease in the DOS at E_F for the compositions of x_{opt}, giving rise to the slight decrease in T_c. Therefore, we conclude that T_s and T_c at x_{opt} are correlated with each other through the strength of the interlayer hybridization.

IV. CONCLUSION

In conclusion, we have systematically studied the relation between the structural phase transition and the superconductivity in $Cu_xIrTe_{2-y}Se_y$. Superconductivity emerges robustly in the vicinity of the structural phase boundary regardless of Se content and T_c minimally decreases with increasing Se content. From the electronic phase diagram for $Cu_xIrTe_{2-y}Se_y$, we have found the strong competition between the Ir-dimer formation and the superconductivity. Furthermore, we have found the important effect of the interlayer hybridization on T_s and T_c at the optimal Cu doping (x_{opt}). T_s increases and T_c decreases by the weakening of interlayer hybridization with increasing y. Specific heat measurements and analyses based on McMillan equation indicate the possible phonon softening and the resultant enhancement of electron-phonon coupling in the vicinity of the structural phase boundary in $Cu_xIrTe_{2-y}Se_y$, especially for the Se-free compound. Our study suggests that the enhanced electron-phonon coupling in the vicinity of the structural phase boundary is a key ingredient for the emergence of superconductivity in doped or intercalated $IrTe_2$ systems.

ACKNOWLEDGMENTS

This study was partly supported by the Japan Society for the Promotion of Science (JSPS) Grants-in-Aid for Scientific Research (No. 25620040 and No. 24224009), the Asahi Glass Foundation, and JST PRESTO program (Hyper-nano-space design toward Innovative Functionality).

[1] J. J. Yang, Y. J. Choi, Y. S. Oh, A. Hogan, Y. Horibe, K. Kim, B. I. Min, and S.-W. Cheong, Phys. Rev. Lett. **108**, 116402 (2012).
[2] S. Pyon, K. Kudo, and M. Nohara, J. Phys. Soc. Jpn. **81**, 053701 (2012).
[3] M. Kamitani, M. S. Bahramy, R. Arita, S. Seki, T. Arima, Y. Tokura, and S. Ishiwata, Phys. Rev. B **87**, 180501(R) (2013).
[4] N. Matsumoto, K. Taniguchi, R. Endoh, H. Takano, and S. Nagata, J. Low Temp. Phys. **117**, 1129 (1999).
[5] G. L. Pascut, K. Haule, M. J. Gutmann, S. A. Barnett, A. Bombardi, S. Artyukhin, T. Birol, D. Vanderbilt, J. J. Yang, S.-W. Cheong, and V. Kiryukhin, Phys. Rev. Lett. **112**, 086402 (2014).
[6] T. Toriyama, M. Kobori, T. Konishi, Y. Ohta, K. Sugimoto, J. Kim, A. Fujiwara, S. Pyon, K. Kudo, and M. Nohara, J. Phys. Soc. Jpn. **83**, 033701 (2014).
[7] H. Cao, B. C. Chakoumakos, X. Chen, J. Yan, M. A. McGuire, H. Yang, R. Custelcean, H. Zhou, D. J. Singh, and D. Mandrus, Phys. Rev. B **88**, 115122 (2013).
[8] K. Kim, S. Kim, K.-T. Ko, H. Lee, J.-H. Park, J. J. Yang, S.-W. Cheong, and B. I. Min, Phys. Rev. Lett. **114**, 136401 (2015).
[9] D. Ootsuki, Y. Wakisaka, S. Pyon, K. Kudo, M. Nohara, M. Arita, H. Anzai, H. Namatame, M. Taniguchi, N. L. Saini, and T. Mizokawa, Phys. Rev. B **86**, 014519 (2012).
[10] Y. S. Oh, J. J. Yang, Y. Horibe, and S.-W. Cheong, Phys. Rev. Lett. **110**, 127209 (2013).
[11] A. F. Fang, G. Xu, T. Dong, P. Zheng, and N. L. Wang, Sci. Rep. **3**, 1153 (2013).
[12] T. Qian, H. Miao, Z. J. Wang, X. Shi, Y. B. Huang, P. Zhang, N. Xu, L. K. Zeng, J. Z. Ma, P. Richard, M. Shi, G. Xu, X. Dai,

Z. Fang, A. F. Fang, N. L. Wang, and H. Ding, New J. Phys. **16**, 123038 (2014).

[13] A. Kiswandhi, J. S. Brooks, H. B. Cao, J. Q. Yan, D. Mandrus, Z. Jiang, and H. D. Zhou, Phys. Rev. B **87**, 121107(R) (2013).

[14] A. Glamazda, K.-Y. Choi, P. Lemmens, J. J. Yang, and S.-W. Cheong, New J. Phys. **16**, 093061 (2014).

[15] S. Jobic, R. Brec, and J. Rouxel, J. Solid State Chem. **96**, 169 (1992).

[16] M. J. Eom, K. Kim, Y. J. Jo, J. J. Yang, E. S. Choi, B. I. Min, J.-H. Park, S.-W. Cheong, and J. S. Kim, Phys. Rev. Lett. **113**, 266406 (2014).

[17] G. L. Pascut, T. Birol, M. J. Gutmann, J. J. Yang, S.-W. Cheong, K. Haule, and V. Kiryukhin, Phys. Rev. B **90**, 195122 (2014).

[18] See Supplemental Material at http://link.aps.org/supplemental/10.1103/PhysRevB.94.134507 for raw data of the Hall resistivity and the specific heat, and the analysis of carrier density for $IrTe_{2-y}Se_y$. We also give the result of the Bloch-Grüneisen fitting for temperature dependence of resistivity for Cu_xIrTe_2.

[19] E. Canadell, S. Jobic, R. Brec, J. Rouxel, and M.-H. Whangbo, J. Solid State Chem. **99**, 189 (1992).

[20] G. Y. Guo and W. Y. Liang, J. Phys. C **19**, 995 (1986).

[21] W. L. Mcmillan, Phys. Rev. **167**, 331 (1968).

[22] R. C. Dynes, Solid State Commun. **10**, 615 (1972).

[23] K. Kudo, M. Takasuga, Y. Okamoto, Z. Hiroi, and M. Nohara, Phys. Rev. Lett. **109**, 097002 (2012).

[24] L. R. Testardi, Rev. Mod. Phys. **47**, 637 (1975).

[25] A. Gauzzi, S. Takashima, N. Takeshita, C. Terakura, H. Takagi, N. Emery, C. Herold, P. Lagrange, and G. Loupias, Phys. Rev. Lett. **98**, 067002 (2007).

[26] Near the structural phase boundary, the absolute values of γ for $Ir_{1-x}Pt_xTe_2$ is probably enhanced due to the strong electron-phonon coupling.

[27] R. A. Jishi and H. M. Alyahyaei, Phys. Rev. B **78**, 144516 (2008).

[28] The enhancement of the Debye temperature by the Se doping can be a factor increasing T_c. It is presumable that this effect tends to mask the effect of the decrease of $\lambda_{\text{el-ph}}$ and DOS on T_c, which would be one of the reasons why the decrease in T_c by the Se doping is so small.